Reduced order modelling and experimental validation of a MEMS gyroscope test-structure exhibiting 1:2 internal resonance

Giorgio Gobat, Valentina Zega, Patrick Fedeli, Luca Guerinoni, Cyril Touzé, Attilio Frangi

Reduced order modelling and experimental validation of a MEMS gyroscope test-structure exhibiting 1:2 internal resonance

Giorgio Gobat[1], Valentina Zega[1], Patrick Fedeli[2], Luca Guerinoni[2], Cyril Touzè[3], Attilio Frangi[1]

[1] Politecnico di Milano, Civil and Environmental Engineering, Milano, Italy

[2] Analog and MEMS group, STMicroelectronics, Cornaredo, Italy

[3] IMSIA, ENSTA Paris, Institut Polytechnique de Paris, Palaiseau, France

*Corresponding Author:

valentina.zega@polimi.it

+390223994213

Abstract

Micro-Electro-Mechanical Systems revolutionized the consumer market for their small dimensions, high performances and low costs. In recent years, the evolution of the Internet of Things is posing new challenges to MEMS designers that have to deal with complex multiphysics systems experiencing highly nonlinear dynamic responses. To be able to simulate a priori and in real-time the behavior of such systems it is thus becoming mandatory to understand the sources of nonlinearities and avoid them when harmful or exploit them for the design of innovative devices. In this work, we present the first numerical tool able to estimate a priori and in real-time the complex nonlinear responses of MEMS devices without resorting to simplified theories. Moreover, the proposed tool predicts different working conditions without the need of ad-hoc calibration procedures. It consists in a nonlinear Model Order Reduction Technique based on the Implicit Static Condensation that allows to condense the high fidelity FEM models into few degrees of freedom, thus greatly speeding-up the solution phase and improving the design process of MEMS devices. In particular, the 1:2 internal resonance experienced in a MEMS gyroscope test-structure fabricated with a commercial process is numerically investigated and an excellent agreement with experiments is found.

Introduction

The spread of Micro-Electro-Mechanical Systems (MEMS) in the consumer world triggered a revolution in gaming, mobile phones and navigation. Similarly, in the near future, the evolution of the Internet of Things in its different declinations will require new generations of sensors and actuators with improved performances, smaller dimensions and innovative working principles. As a consequence, MEMS designers more and more frequently will have to deal with complex mechanical structures exhibiting nonlinear dynamic behaviors[1-2].

Among others, MEMS gyroscopes represent a meaningful example of such a trend. They are electro-mechanical systems able to measure the angular rate by exploiting the Coriolis force. To guarantee a correct functioning, where at least two modes are coupled through the Coriolis force, and to satisfy the strict requirements on the footprint, the mechanical structure is usually very complex, i.e. made by folded springs and rigid masses. Nonlinear phenomena often arise[3-8] but are difficult to decipher.

Among the wide variety of nonlinear phenomena arising in MEMS devices, internal resonance, i.e. when two or more modes get nonlinearly coupled and exchange energy, is attracting increasing interest for its potential benefits on the performances of MEMS devices[2,9-12]. It has been demonstrated that thanks to internal resonance it is indeed possible *(i)* to stabilize the oscillation frequency of non-linear self-sustaining micromechanical resonators[13], *(ii)* to redistribute and store mechanical energy among vibrational modes and coherently transfer it back to the principal one when the external excitation is off[14] and *(iii)* to tune the quality factor Q of the driven mode over a wide range[15-16]. Moreover, internal resonance has been recently employed in MEMS gyroscopes

as a new and very promising detection technique of angular rate signals[17] and to design innovative MEMS bandpass filters[18].

In view of its high potentiality for the design of innovative and high-end MEMS devices, internal resonance has been analyzed theoretically[19] and experimentally verified on a variety of simple MEMS structures[20-24], ranging from arch resonators[25-27] to micro-mirrors[28]. In most cases, the coefficients of Reduced Order Models (ROMs) are obtained from simplified electro-structural theories[26,29] or are calibrated on experimental data[23]. Despite the great interest of the topic, a general a priori simulation tool that could predict in real-time the nonlinear dynamic behavior of complex MEMS structures like e.g. gyroscopes under different actuation conditions, is still missing. Such a tool would also dramatically improve the design process and pave the way to a new class of sensors/actuators experiencing complex nonlinear dynamic phenomena.

Numerical methods able to simulate the Full Order Model (FOM) have been proposed as a generalization of simplified appoaches[30], but their computational cost remains a major issue especially if complex MEMS structures are considered. Dedicated Harmonic Balance techniques or shooting procedures are indeed overwhelmingly complex and time consuming[31-32].

As a consequence, the focus has been set on the generation of nonlinear ROMs starting e.g. from large FEM models that might reshape the governing equations into a nonlinear, dynamical system featuring a much lower dimensionality, yet able to capture the physical features of the problem[29,33-35]. The Stiffness Evaluation Procedure (STEP) in its various variants[33] assumes a trial subspace spanned by a set of linear modes which however must also include all the coupled high-frequency modes that are often difficult to identify[36-37]. The Proper Orthogonal Decomposition (POD)[38] is also based on a linear trial space but this is generated from a set of FOM snapshots employing

Singular Value Decomposition, thus allowing to identify all the relevant contributions automatically. A different approach is taken by the implicit condensation and expansion (ICE) method[39-41] which defines a small set of master modes and assumes a quasi-static coupling with the high frequency contributions (slave modes). Also modal derivatives (MD)[42-44] have been introduced with the aim of accounting for the amplitude dependence of modes. ICE and MD are indeed very accurate when a slow/fast separation between the frequencies of the master and slave modes exist[45-46]. Recently, Nonlinear Normal Modes (NNMs) have received considerable attention as a technique for generating ROMs. Initially defined as a vibration in unison of the system[47-49], they have been later extended by the notion of invariant manifold[50] and of spectral submanifold (SSM)[51-52]. However, only very recently efficient approaches have been proposed for the computation of invariant manifolds for large FEM models[53-54], but applications have been limited so far to mechanical structures with geometrical nonlinearities and no multiphysics coupling.

In this work, we elaborate on the Implicit Condensation approach based on static modal loadings recently tailored by the authors for simple MEMS structures[41]. In particular, the ICE applies to structures which undergo transformations which are no-longer infinitesimal, but still moderate. The approach has been verified on a double-ended tuning fork resonator experiencing both geometric, electrostatic and damping nonlinearities[55], and represents a fast a priori multiphysics simulation tool able to reproduce the nonlinear dynamics caused by the interaction of two modes of a complex MEMS gyroscope test-structure without the need of calibration procedures. To the authors best knowledge this represents the first fast numerical predictive tool able to simulate a priori the internal resonance phenomenon including bifurcations of the periodic response in a complex structure and in general, the nonlinear dynamic behavior of MEMS devices. Numerical

results are compared with experimental data and an excellent agreement is achieved for different actuation conditions, thus proving the versatility and the predictivity of the proposed tool.

Results

MEMS gyroscope test-structure

A schematic view of the MEMS gyroscope test-structure employed in this work is reported in Fig. 1a, close-up views and geometrical dimensions are instead reported in the Supplementary Information for the sake of clarity. The mechanical structure is constituted by four masses and several folded springs that provide the suspension of the device and the coupling of the masses with a central auxiliary component. The gyroscope test-structure is fabricated through the Thelma process of STMicroelectronics in polysilicon (E = 167GPa, υ = 0.22, ρ = 2330 Kg/m^3) and has an overall footprint of 1.5mm x 1.3mm x 24μm. Comb finger and parallel plate electrodes allow for the in-plane actuation/readout, while electrodes located on the substrate are employed for the out-of-plane actuation/readout. In Fig. 1b-c, two modes of the MEMS gyroscope test-structure are reported: they will be referred to in the following as roll mode (Fig. 1b) and spurious roll mode (Fig. 1c). Their natural frequencies are computed through a FEM modal analysis and read f_1 = 22522 Hz and f_2 = 43386 Hz, respectively.

1:2 internal resonance between the two modes can be triggered by driving the roll mode through the electrodes on the substrate. The two linear natural frequencies have an initial ratio of 1.926, which evolves to almost exactly 2 as the applied electrostatic bias increases and due to the electrostatic nonlinearities given by the parallel-plate electrostatic scheme[55].

ROM based on Implicit Static Condensation

A numerical FOM made by discretizing the geometry of the MEMS gyroscopes test-structure with quadratic pentahedrons, properly distributed so as to have at least two elements in the spring thickness, consists of around 2.5 million of degrees of freedom which become 17 million if electro-mechanical coupling is considered. This makes any direct numerical simulation computationally unaffordable especially if complex nonlinear dynamic phenomena such as the 1:2 internal resonance are investigated. As an example, to simulate the nonlinear dynamic response of the MEMS quad-mass structure through fully coupled time domain analyses in COMSOL Multiphysics v.5.6, we estimate around a year of simulation with a standard workstation (AMD Ryzen 9 5950X, 16 Cores, 128Gb RAM).

The implicit static condensation method validated by the authors on simple structures[41,55] is here applied to reduce the system to two degrees of freedom (i.e. the amplitudes of the two master roll and spurious-roll modes), thus dramatically reducing the computational effort without losing accuracy and physical meaning (see Methods Section).

By considering a constant Direct Current (DC) voltage V_{DC} on the MEMS gyroscope test-structure proof masses and an Alternate Current (AC) signal $V_{AC} \ll V_{DC}$ at an angular frequency ω close to the one of the roll mode on the electrodes on the substrate, the resulting nonlinear system describing the dynamics of the device reads:

$$\ddot{q}_1 + \frac{\omega_{01}}{Q_1}\dot{q}_1 + \beta_1(q_1, q_2) - \check{F}_{e1_1}(q_1, q_2)\epsilon_0 V_{DC}^2 = 2\epsilon_0 V_{DC} V_{AC} \check{F}_{e2_1}(q_1, q_2) \sin \omega t, \quad (1)$$

$$\ddot{q}_2 + \frac{\omega_{02}}{Q_2}\dot{q}_2 + \beta_2(q_1, q_2) - \check{F}_{e1_2}(q_1, q_2)\epsilon_0 V_{DC}^2 = 0, \quad (2)$$

where ϵ_0 is the vacuum permittivity, q_i is the modal coordinate, Q_i is the quality factor, $\omega_{0i} = 2\pi f_i$ is the natural pulsation, $\beta_i(q_1, q_2)$ is the nonlinear mechanical force and $\check{F}_{e1_i}(q_1, q_2)$ is a time independent nonlinear electrostatic force for the *i*-th mode, with *i*=1 for the roll mode and *i*=2 for the spurious roll mode. $\check{F}_{e2_1}(q_1, q_2)$ is the time dependent nonlinear electrostatic force that acts

on the driven roll mode. In the following, $Q_1 = 2400$ and $Q_2 = 3480$ according to the simplified numerical tool[56] proposed by the authors to compute fluid damping in MEMS resonant structures working in low pressure conditions such as in this case. Note that a nonlinear quality factor can in principle be also considered in the case of very large displacements of the proof mass with respect to the air gap between it and the fixed electrodes[55].

For the sake of simplicity, we approximate $\beta_i(q_1, q_2)$, $\check{F}_{e1_i}(q_1, q_2)$ and $\check{F}_{e2_1}(q_1, q_2)$ with a complete third order polynomial whose coefficients are reported in the Supplementary Information. Once the voltage levels are fixed, Eqs. (1)-(2) are solved through numerical continuation, using the package MANLAB[57] that implements a combination of Harmonic Balance (HB) with an asymptotic numerical method (ANM) for path-following. The nonlinear frequency response of the roll mode in terms of amplitude and phase is reported in continuous light blue line in Fig. 2 for a V_{DC}= 4.28V and a V_{AC} = 3.16mV. For this actuation condition, the model correctly reproduces the activated 1:2 internal resonance as demonstrated by the characteristic shape of the frequency response made with two peaks and by the presence of a quasi-periodic/chaotic region (see green path in Fig.2(a) of Supplementary Information) delimited by Neimark-Sacker bifurcations (dark blue stars in Fig.2) in the central region of the spectrum58. Red stars represent the Saddle-Node bifurcations predicted by the ROM model and delimit the unstable part of the solution branch (see red path in Fig.2(a) of Supplementary Information). To further validate the adequacy of the proposed ROM, in the Supplementary Information we report the comparison between the curves obtained through the full ROM here proposed and the ones analytically derived through the Multiple Scale Method[58] from a simplified ROM based on the coefficients numerically extracted through the Implicit Condensation Method.

In Fig.2, numerical curves in terms of displacements obtained by integrating Eqs. (1)-(2) are converted in terms of current as detailed in Zega et al.[55] to simplify the comparison with experimental data.

Experimental results

In order to validate the proposed simulation tool, the experimental frequency response of the MEMS gyroscope test-structure is measured in the same actuation condition previously considered for the theoretical model: V_{DC}= 4.28V and V_{AC} = 3.16 mV. Experimental curves are reported in orange dashed lines in Fig.2 and well agree with the numerical predictions. Note that the jumps of the experimental upward frequency sweep shown in Figs.2(a),(c) are in a satisfactory agreement with the Saddle-Node bifurcations (red stars) predicted by the models (see Fig. 2(a) of Supplementary Information). Moreover, in the close-up views of Figs.2(b),(d), it is evident that the Neimark-Sacker bifurcations predicted by the ROM correctly delimit the experimental quasi-periodic region, thus further proving the accuracy of the proposed a priori simulation tool.

Additional experimental curves measured for a V_{AC} = 3.16 mV and different levels of V_{DC} are reported in dashed-lines in Fig.3 together with corresponding numerical predictions. Only experimental upward frequency sweeps are reported for the sake of clarity and all the curves, both numerical and experimental, are normalized with the maximum amplitude of the hardening peak of the experimental curve obtained for V_{DC}= 4.28V and V_{AC} = 3.16 mV. This value corresponds to an out-of-plane maximum displacement of the proof masses of 71nm. The maximum displacement experienced by the proof masses in this experimental campaign is then in the order of a couple of hundreds of nanometers (i.e. orange curve in Fig.3a), which is fully compatible with a stable operation of the device far from pull-in instabilities (the gap between the masses and the underlying electrodes is of 1.2μm) and with the assumption of moderate transformations required

by the proposed ICE method. In the inset of Fig.3(b), the evolution of the resonant frequency of the roll mode for different V_{DC} is reported and compared with half the resonant frequency of the spurious roll mode, highlighting the strong link between the nonlinear dynamic behavior of the structure under study and the ratio between the resonant frequencies of the two coupled modes.

A good agreement in terms of amplitude and phase, e.g. experimental jumps in proximity of Saddle-Node bifurcations predicted by the proposed MOR (see Fig. 2(a) of Supplementary Information), is found for all the DC-voltage levels, thus proving the predictive ability of the simulation tool. It is worth noting that the proposed ROM is able to catch the nonlinear dynamic response of the MEMS gyroscope test structure under different actuating conditions without any need of ad-hoc calibration of the coefficients. This make this simulation approach extremily versatile and general.

Discussion

The proposed ROM based on implicit static condensation is able to accurately and ab-initio reproduce the complex nonlinear dynamics of a MEMS gyroscope test-structure undergoing 1:2 internal resonance including bifurcations of the periodic response. The obtained two degrees of freedom model accounts for the multi-physics nature of the problem and does not require any calibration of the parameters: nonlinear coefficients come indeed exclusively from numerical simulations and can be estimated without the need of experimental data. Moreover, thanks to the reduction of the number of degrees of freedom of the system, simulations run almost real-time and are thus very helpful for design purposes and experimental data post-processing.

This technique represents, to the authors' best knowledge, the first tool able to estimate a priori and in real-time the nonlinear dynamics of a complex multiphysics system like a MEMS gyroscope test-structure under different actuation conditions.

MEMS designers and the MEMS industry in general, will strongly benefit of such tool since it will simplify the understanding of experimental data and the design process of complex nonlinear MEMS devices.

Methods

Implicit static condensation

The implicit static condensation is based on the assumption that it is possible to describe the steady state non-linear oscillation of a resonator as a combination of few master modes (MM). The dynamics of the ROM is described by a stress manifold obtained by implicitely condensing the effects of higher order modes that locally modify the internal forces and thus the global stiffness of the system[42]. For the case under study where two modes interact through the internal resonance, this method allows to formulate a ROM where the active degrees of freedom are the modal coordinates q_i of the roll and the spurious roll modes associated to the maximum out-of-plane displacement of the proof masses. Let $\psi_i(x)$ denote the displacement field of the *i*-th MM, mass normalized, the non-linear elastic force manifold is evaluated by statically forcing the structure with suitable body forces *F* which are proportional to $\psi_1(x)$ and $\psi_2(x)$: $F = \beta_1\psi_1(x) + \beta_2\psi_2(x)$. The motivation for this choice, apart from simplicity, is that these loads are a very good approximation of inertia forces occurring during the steady state oscillation. Once the body forces are defined, a series of static non-linear analyses are run spanning the (β_1, β_2) space. The range of the load-multipliers (β_1, β_2) is prescribed so as to cover the expected displacements of the structure, e.g. maximum out-of-plane displacements allowed by the gap between the proof masses and the underlying substrate. Let $(q_1(\beta_1, \beta_2), q_2(\beta_1, \beta_2))$ denote the solution for a given (β_1, β_2), we invert such relations and we obtain the terms $(\beta_1(q_1, q_2), \beta_2(q_1, q_2))$ of Eqs. (1)-(2).

A similar procedure is adopted to determine the electrostatic nonlinear manifold of the ROM. This represents a quasi-static approach which assumes that the dynamics of electromagnetic forces is much faster than the frequency of oscillation of the resonators, which is verified in the case of the MEMS under consideration. We then suppose that the gyroscope vibrates according to a combination of the two main modes, i.e. roll and spurious roll modes, and we update the coordinates of the conductor surfaces, i.e. surfaces of the proof masses of the gyroscope test-structure that face the underlying electrodes employed for actuation/readout, as $x + \psi_1 q_1 + \psi_2 q_2$, being x the initial position of the conductor surfaces. The map of the charge surface density $\sigma(x, q_1, q_2)$ caused by the interaction between the conductor surfaces with the underlying electrodes, is then computed as a function of (q_1, q_2) through integral equations accelerated with fast multipole methods[59]. Once the charge surface density is available, the nonlinear load participation factor is computed as:

$$F_{e_i} = \int_S \frac{\sigma^2}{2} \psi_{n_i} \, dS \approx \epsilon_0 \check{F}_{e1_i} V_{DC}^2, \tag{3}$$

where $\psi_{n_i} = \psi_i \cdot n$ is the projection of the modal shape function ψ_i along the outward unit normal vector on the conductor surface and S is the surface portion of the proof masses that faces the underlying electrodes. An analogous procedure[55] allows us to determine the nonlinear amplitude of the forcing term $\check{F}_{e2_1}(q_1, q_2)$ in Eqs. (1)-(2).

Experimental set-up

The MEMS is bonded to a ceramic carrier and then connected to a Plastic Circuit Board (PCB) as shown in Fig. 4a. Electrostatic actuation of the roll mode is provided through two power suppliers (Fig. 4b-c): the Agilent E3631A provides the DC voltage while AC signal is generated through the Agilent AG4395A. The output current measured on the electrodes on the substrate is amplified through the Signal amplifier SRS model SR570 (Fig. 4d) and read in the frequency domain through

the Agilent AG4395A (Fig. 4c). A LabView script (Fig. 4e) acquires the output and corrects the AC signal to guarantee a close-loop control of the circuit.

References

1. C. Comi et al Non-linear mechanics in resonant inertial micro sensors *Int. J. of Non-Linear Mech*. **120** 103386 (2020)
2. O. Shoshani et al Resonant Modal Interactions in Micro/nano-mechanical structures *Nonlinear Dynamics* in press (2021)
3. S.H. Nitzan et al Self-induced parametric amplification arising from nonlinear elastic coupling in a micromechanical resonating disk gyroscope *Sci. Rep.* **5** 9036 (2015)
4. P. Polunin et al Self-induced parametric amplification in ring resonating gyroscopes, *Int. J. Non-Linear Mech.* **94** 300–308 (2017)
5. S.H. Nitzan et al Countering the Effects of Nonlinearity in Rate-Integrating Gyroscopes *IEEE Sensors J.* **16** (10) 3556–3563 (2016)
6. U. Nabholz et al Nonlinear Dynamical System Model for Drive Mode Amplitude Instabilities in MEMS Gyroscopes *2019 IEEE Int. Symposium on Inertial Sensors and Syst. (INERTIAL)*, Naples, FL, USA, 1-4 (2019)
7. V. Zega et al Hardening, Softening, and Linear Behavior of Elastic Beams in MEMS: An Analytical Approach. *J. Microelectromech. Syst*. **28**(2) 189-198 (2019)
8. G. Gobat et al Interpolation based reduced order modelling for non-linearities in MEMS *IEEE Sensors 2020* online (2020)
9. A.D. Shaw et al Periodic responses of a structure with 3:1 internal resonance *Mech. Syst. And Signal Processing* **81** 19-34 (2016)
10. F. K. Alfosail et al Theoretical and Experimental investigation of two-to-one internal resonance in MEMS arch resonators *J. Computational and Nonlinear Dynamics* **14**(1) 011001 (2018)
11. K.R. Qalandar et al Frequency division using a micromechanical resonance cascade *Appl. Phys. Lett*. **105** 244103 (2014)

12. A. Sarrafan et al Development and characterization of an H-shaped microresonator exhibiting 2:1 internal resonance *J. Microelectromech. Syst.* **26**(5) 993-1001 (2017)
13. D. Antonio et al Frequency stabilization in nonlinear micromechanical oscillators *Nat. Commun.* **8** 15523 (2017)
14. C. Chen et al Direct observation of coherent energy transfer in nonlinear micromechanical oscillators *Nat. Commun.* **8** 15523 (2017)
15. Ian B. Flader et al Tunable quality factor through 1:1 modal coupling in a disk resonator, 2015 IEEE SENSORS, Busan, Korea (South) 1-4 (2015)
16. A. Keskekler et al Tuning nonlinear damping in graphene nanoresonators by parametric-direct internal resonance *Nature Comm*. **12** 1099 (2021)
17. A. Sarrafan et al A nonlinear rate microsensor utilising internal resonance, *Sci. Rep.* **9** 8648 (2019)
18. A.Z. Hajjaj et al Mode coupling and nonlinear resonances of MEMS arch resonators for bandpass filters *Sci. Rep.* **7** 41820 (2017)
19. A. H. Nayfeh Nonlinear Interactions: analytical, computational and experimental methods *Wiley* (2000)
20. R.B. Karabalin et al Nonlinear dynamics and chaos in two coupled nanomechanical resonators *Physical Review B* **79**(16) 165309 (2009)
21. L. Ruzziconi et al Two-to-one internal resonance in the higher-order modes of a MEMS beam: experimental investigation and theoretical analysis via local stability theory *Int. J. Non-Linear Mech*. **129** 103664 (2021)
22. A. Vyas et al A microresonator design based on nonlinear 1: 2 internal resonance in flexural structural modes *J. of Microelectromech. Syst.* **18**(3) 744-762 (2009)
23. D.A. Czaplewski Bifurcation diagram and dynamic response of a MEMS resonator with a 1:3 internal resonance *Appl. Phys. Lett*. **114**, 254104 (2019)
24. A. Sarrafan et al Analytical Modeling and Experimental verification of Nonlinear Mode Coupling in a Decoupled Tuning Fork Microresonator *J. Microelectromech. Syst*. **27**(3) 398-406 (2018)
25. A.Z. Hajjaj et al Multiple internal resonance in MEMS arch resonators *Physics Letters A* **382** 3393-3398 (2018)
26. A. Hajjaj et al Two-to-one internal resonance of MEMS arch resonators *Int. J. of Non-Linear Mech.* **107** 64–72 (2018)

27. Q. Bi et al Analysis of non-linear dynamics and bifurcations of a shallow arch subjected to periodic excitation with internal resonance. *J. Sound Vibration* **233**(4) 553-567 (2020)
28. U. Nabholz et al Spontaneous Parametric Down-Conversion Induced by Non-Degenerate Three-Wave Mixing in a Scanning MEMS Micro Mirror *Sci. Rep.* **9** 3997 (2019)
29. M. Younis et al A reduced-order model for electrically actuated microbeam-based MEMS *J. of Microelectromech. Syst.* **12** (5) 672–680 (2003)
30. M. Putnik et al Predicting the resonance frequencies in geometric nonlinear actuated MEMS *J. Microelectromech. Syst.* **27** (6) 954–962 (2018)
31. G. Kerschen et al Nonlinear normal modes, Part I: A useful framework for the structural dynamicist *Mech. Syst. and signal processing* **23.1** 170-194 (2009)
32. L. Renson et al Numerical computation of nonlinear normal modes in mechanical engineering *J. of Sound and Vibration* **364** 177-206 (2016)
33. M.P. Mignolet et al A review of indirect/non-intrusive reduced order modeling of nonlinear geometric structures *J. Sound and Vibration* **332**(10) 2437-2460 (2013)
34. B. Besselink et al A comparison of model reduction techniques from structural dynamics, numerical mathematics and systems and control *J. sound and vibration* **332**(19) 4403-4422 (2013)
35. F. Negri et al Efficient model reduction of parametrized systems by matrix discrete empirical interpolation *J. Computational Physics* **303** 431-454 (2015)
36. A. A. Muravyov et al Determination of nonlinear stiffness with application to random vibration of geometrically nonlinear structures *Computers & Structures* **81**(15) 1513–1523 (2003)
37. A. Vizzaccaro et al Non-intrusive reduced order modelling for the dynamics of geometrically nonlinear flat structures using three-dimensional finite elements *Computational Mechanics* **66** 1293-1319 (2020)
38. G. Kerschen et al The method of proper orthogonal decomposition for dynamical characterization and order reduction of mechanical systems: an overview *Nonlinear dynamics* **41.1-3** 147-169 (2005)
39. J. J. Hollkamp et al Reduced-order models for non-linear response prediction: Implicit condensation and expansion *J. of Sound and Vibration* **318** 1139–1153 (2008)
40. E. Nicolaidou et al Indirect reduced-order modelling: using nonlinear manifolds to conserve kinetic energy *Proc. R. Soc. A*. **476** 20200589 (2021)

41. A. Frangi et al Reduced order modelling of the non-linear stiffness in MEMS resonators. *Int. J. Non-Linear Mech.* **116** 211-218 (2019)
42. S. R. Idelsohn et al A reduction method for nonlinear structural dynamic analysis. *Computer Methods in Applied Mech. and Eng.* **49** (3) 253 – 279 (1985)
43. O. Weeger et al On the use of modal derivatives for nonlinear model order reduction *Int. J. for Numerical Methods in Eng.* **108**(13) 1579–1602 (2016)
44. S. Jain et al A quadratic manifold for model order reduction of nonlinear structural dynamics *Computers & Structures* **188** 80–94 (2017)
45. A. Vizzaccaro et al Comparison of nonlinear mappings for reduced-order modelling of vibrating structures: normal form theory and quadratic manifold method with modal derivatives *Nonlinear Dynamics* **103** 3335-3370 (2021)
46. Y. Shen et al Reduced order models for geometrically nonlinear structures: assessment of implicit condensation in comparison with invariant manifold approach *European J. Mechanics: A/Solids* **86** 104165 (2021)
47. C. Touzè Normal form theory and nonlinear normal modes: Theoretical settings and applications *Modal analysis of nonlinear mechanical systems* Springer, Vienna, 75-160 (2014)
48. C. Touzè et al Nonlinear normal modes for damped geometrically nonlinear systems: Application to reduced-order modelling of harmonically forced structures *J. of sound and vibration* **298.4-5** 958-981 (2006)
49. D. Jiang et al Nonlinear normal modes for vibratory systems under harmonic excitation *J. of sound and vibration* **288.4-5** 791-812 (2005)
50. S.W. Shaw An invariant manifold approach to nonlinear normal modes of oscillation *J. Nonlinear Science* **4** 419-448 (1994)
51. G. Haller et al Nonlinear normal modes and spectral submanifolds: existence, uniqueness and use in model reduction *Nonlinear Dyn.* **86** 1493-1534 (2016)
52. S. Ponsioen et al Automated computation of autonomous spectral submanifolds for nonlinear modal analysis *J. Sound and Vibration* **420** 269-295 (2018)

53. A. Vizzaccaro et al Direct computation of nonlinear mapping via normal form for reduced-order models of finite element nonlinear structures, *Computer Methods in Applied Mechanics and Engineering*, arXiv preprint arXiv:2009.12145 (2020)
54. A. Opreni et al Model Order Reduction based on Direct Normal Form: Application to Large Finite Element MEMS Structures Featuring Internal Resonance, *Nonlinear Dynamics*, arXiv preprint arXiv:2103.10545 (2021)
55. V. Zega et al Numerical modelling of non-linearities in MEMS resonators *J. Microelectromech. Syst.* **29**(6) 1443-1454 (2020)
56. P. Fedeli et al Near vacuum gas damping in MEMS: Simplified modeling *J. Microelectromech. Syst.* **26**(3) 632–642 (2017)
57. L. Guillot et al A Taylor series-based continuation method for solutions of dynamical Syst. *Nonlinear Dyn.* **98**(4) 2827-2845 (2019)
58. G. Gobat et al Backbone Curves, Neimark-Sacker Boundaries and Appearance of Quasi-Periodicity in Nonlinear Oscillators: Application to 1:2 Internal Resonance and Frequency Combs in MEMS *Meccanica* (2021) doi: 10.1007/s11012-021-01351-1
59. A. Frangi et al Multipole BEM for the evaluation of damping forces on MEMS *Comput. Mech*. **37**(1) 24–31 (2005)

Authors contributions

G.G., V.Z., C.T. and A.F. coinceived the idea and developed the supporting theory. G.G. performed numerical analyses, L.G. and P.F. perform experimental tests. V.Z., C.T. and A.F. oversaw the research, provide guidance and discussed the results and implications at all stages. V.Z. wrote the manuscript and all authors edited the manuscript.

Competing interests

The authors declare no competing interests.

Additional information

Supplementary information is available for this paper

1:2 internal resonance with Neimark-Sacker bifurcations in a MEMS gyroscope test-structure: reduced order modelling and experimental validation

Giorgio Gobat[1], Valentina Zega[1,*], Patrick Fedeli[2], Luca Guerinoni[2], Cyril Touzè[3], Attilio Frangi[1]

[1] Politecnico di Milano, Civil and Environmental Engineering, Milano, Italy

[2] Analog and MEMS group, STMicroelectronics, Cornaredo, Italy

[3] IMSIA, ENSTA Paris, Institut Polytechnique de Paris, Palaiseau, France

*Corresponding Author:

valentina.zega@polimi.it

+390223994213

Supplementary Information

1. MEMS quad-mass gyroscope test structure geometry

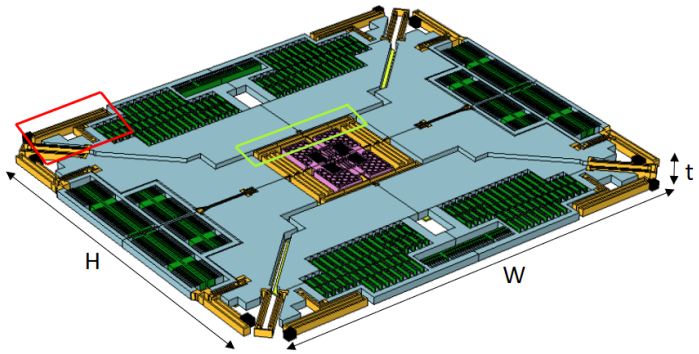

H	1.3 mm
W	1.5 mm
t	24 µm
L	254 µm
h	103 µm
s	4.8 µm
L1	353 µm
s1	4.8 µm

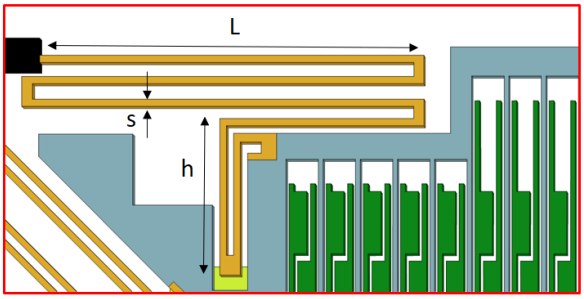

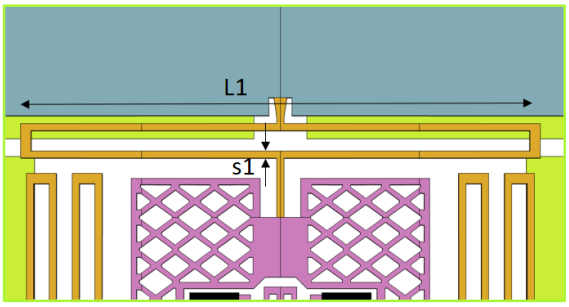

Figure 1: Schematic view of the MEMS test structure. Two close-up views and geometric dimensions are also reported for the sake of clarity.

2. Implicit Condensation Method: nonlinear mechanical and electrostatic forces

In this work, the nonlinear mechanical and electrostatic forces (eqs. (1)-(2) of the paper) computed through the Implicit Condensation Method are interpolated with a complete third order polynomial of the general form:

$$P(q_1, q_2) = c_0 + c_1 q_1 + c_2 q_2 + c_3 q_1^2 + c_4 q_1 q_2 + c_5 q_2^2 + c_6 q_1^3 + c_7 q_1^2 q_2 + c_8 q_1 q_2^2 + c_9 q_2^3.$$

The coefficients utilized for the different contributions are reported in Table 1. It is worth noting that such coefficients do not depend on the V_{DC} and V_{AC} values and thus able to describe the nonlinear dynamics of the MEMS gyroscope test-structure under different actuating conditions.

	$\boldsymbol{\beta_1(q_1,q_2)}$ [μN]	$\boldsymbol{\beta_2(q_1,q_2)}$ [μN]	$\boldsymbol{\breve{F}_{e1_1}(q_1,q_2)}$ [μN μm/V² pF]	$\boldsymbol{\breve{F}_{e1_2}(q_1,q_2)}$ [μN μm/V² pF]	$\boldsymbol{\breve{F}_{e2_1}(q_1,q_2)}$ [μN μm/V² pF]
$\boldsymbol{c_0}$	$3.67\ 10^{-6}$	$-2.24\ 10^{-6}$	-0.08555	-284.389	-476.658
$\boldsymbol{c_1}$	0.020024	$-2.38\ 10^{-6}$	11.23799	0.087044	5.565844
$\boldsymbol{c_2}$	$-2.33\ 10^{-6}$	0.074312	0.087168	9.511499	4.334514
$\boldsymbol{c_3}$	$5.19\ 10^{-11}$	$-1.75\ 10^{-8}$	$-2.68\ 10^{-5}$	-0.071	-0.04597
$\boldsymbol{c_4}$	$-1.49\ 10^{-8}$	$1.41\ 10^{-8}$	-0.1424	$-3.65\ 10^{-5}$	-0.07233
$\boldsymbol{c_5}$	$-5.80\ 10^{-9}$	$1.14\ 10^{-9}$	$-2.12\ 10^{-5}$	-0.03227	-0.02853
$\boldsymbol{c_6}$	$-3.05\ 10^{-11}$	$-1.69\ 10^{-12}$	0.000826	$7.66\ 10^{-7}$	0.000413
$\boldsymbol{c_7}$	$-3.80\ 10^{-12}$	$-2.83\ 10^{-10}$	$1.22\ 10^{-6}$	0.001439	0.000899
$\boldsymbol{c_8}$	$-4.01\ 10^{-10}$	$-5.49\ 10^{-12}$	0.001488	$9.37\ 10^{-7}$	0.000734
$\boldsymbol{c_9}$	$-9.80\ 10^{-12}$	$-2.03\ 10^{-9}$	$4.41\ 10^{-7}$	0.000497	0.000263

Table 1: Coefficients of the polynomial expansion of the mechanical and electrostatic nonlinear forces obtained through the Implicit Condensation Method.

3. Nonlinear frequency response in presence of 1:2 internal resonance

In the presence of a 1:2 internal resonance, the frequency response of each of the two coupled modes takes the peculiar shape reported in Fig.2. As the two peaks of the frequency response are strongly nonlinear, i.e. one hardening and one softening, Saddle-Node bifurcations (red stars in Fig.2) are also present to delimit their unstable branches (red path in Fig.2). Unstable branches cannot be followed experimentally using a standard set-up and, as a consequence, jumps are expected in the proximity of Saddle-Node bifurcations. The experimental frequency response will be then strongly dependent on the sweep direction as shown by arrows in Figs.2(a)-(b).

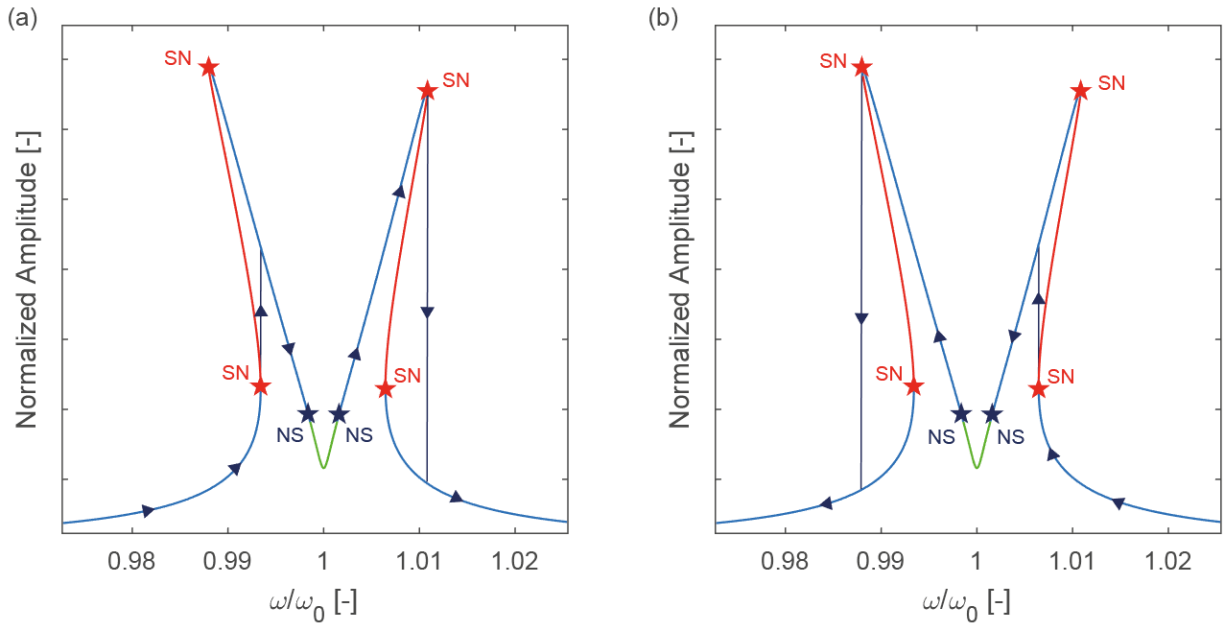

Figure 2: Nonlinear frequency response in presence of a 1:2 internal resonance. (a) Upward and (b) downward frequency sweeps.

It is worth mentioning that a variable-phase feedback loop on the resonator would allow to track the response beyond the critical bifurcation regime[1] but the implementation of such control circuit is outside the scope of the present work.

Finally, Neimark-Sacker bifurcations (dark blue stars) also appear, thus delimiting the quasi-periodic region (green path in Fig.2) where the steady-state periodic response is no longer stable and bifurcates into a quasi-periodic response. This latter is no longer characterized by a single frequency, given by the external excitation, but also by an incommensurate smaller frequency that modulates the response[2]. Moreover, within this region, the quasi-periodic regime can further bifurcate into a nearly chaotic response that is extremely hard to predict. Neimark-Sacker bifurcations have been predicted numerically as illustrated in the body of the paper.

4. Simplified analytical model

In order to further validate the numerical results obtained from the ROM with specific reference to the prediction of the quasi periodic region, we discuss an analytical model obtained starting from the normal form theory. Considering nonlinear terms up to the quadratic order for the sake of simplicity, the normal form for the 1:2 internal resonance reads[2]:

$$\begin{aligned} \ddot{q}_1 + 2\mu_1\dot{q}_1 + (\omega_{01}^2 - \breve{\boldsymbol{F}}_{\boldsymbol{e1_1c_1}}\epsilon_0 V_{DC}^2)\delta_{1c_1} q_1 + \left(\boldsymbol{\beta}_{\boldsymbol{1,c_4}} - \breve{\boldsymbol{F}}_{\boldsymbol{e1_1c_4}}\epsilon_0 V_{DC}^2\right) q_1 q_2 &= 2\,\breve{\boldsymbol{F}}_{\boldsymbol{e2_1c_0}}\epsilon_0 V_{DC} V_{AC}\cos\omega t \\ \ddot{q}_2 + 2\mu_2\dot{q}_2 + (\omega_{02}^2 - \breve{\boldsymbol{F}}_{\boldsymbol{e1_2c_1}}\epsilon_0 V_{DC}^2)\delta_{2c_1} q_2 + \left(\boldsymbol{\beta}_{\boldsymbol{2,c_3}} - \breve{\boldsymbol{F}}_{\boldsymbol{e1_2c_3}}\epsilon_0 V_{DC}^2\right) q_1^2 &= 0, \end{aligned} \tag{1}$$

where q_i are the modal coordinates, $2\mu_i$ the damping coefficients, ω the external forcing pulsation and δ_{ic_1} are almost unitary correction factors used to force a perfect match of the eigenfrequencies of the model with the measured ones. The other symbols have the same meaning used in the Implicit Condensation approach proposed in the paper.

Coefficients of the analytical model (1) are retrieved from the proposed numerical Implicit Condensation Method (see Table 1 of Supplementary Information) and summarized in Table 2.

As shown in a recent contribution[2], starting from the normal form (1), it is possible to estimate in a closed form both the frequency response curve of the two-dofs system and the Neimark-Sacker boundary curve, i.e. locus of the bifurcation points in the parameters space.

A comparison between the frequency response curve obtained through the full ROM studied in the paper and the simplified analytical model is shown in Fig.3 in terms of amplitude of the modal coordinate of the driven roll mode for a V_{AC}=3.16mV and a V_{DC}=4.28V. Red and black stars denote Saddle-Node and Neimark-Sacker bifurcations identified through the numerical model, while the green dashed line represents the analytical Neimark-Sacker boundary curve estimated from eq. (1) through the Multiple Scales Method[2].

Parameter	Value	Units
$\boldsymbol{\omega_{01}^2}$	0.020024	$\mu N/\mu m$
$\boldsymbol{\omega_{02}^2}$	0.074312	$\mu N/\mu m$
$\breve{\boldsymbol{F}}_{\boldsymbol{e1_1c_1}}$	11.23799	$\mu N/\ \mu m\ V^2\ pF$
$\breve{\boldsymbol{F}}_{\boldsymbol{e1_2c_1}}$	9.511499	$\mu N/\ \mu m\ V^2\ pF$
$\breve{\boldsymbol{F}}_{\boldsymbol{e1_1c_4}}$	-0.1424	$\mu N/\ \mu m^2\ V^2\ pF$
$\breve{\boldsymbol{F}}_{\boldsymbol{e1_2c_3}}$	-0.071	$\mu N/\ \mu m^2\ V^2\ pF$
$\boldsymbol{\beta_{1,c_4}}$	$-1.49\ 10^{-8}$	$\mu N/\mu m^2$
$\boldsymbol{\beta_{2,c_3}}$	$-1.75\ 10^{-8}$	$\mu N/\mu m^2$
$\breve{\boldsymbol{F}}_{\boldsymbol{e2_1c_0}}$	-476.658	$\mu N/V^2\ pF$
$\boldsymbol{\delta_{1c_1}}$	0.99948	-
$\boldsymbol{\delta_{2c_1}}$	0.99994	-
$\boldsymbol{\mu_1}$	$2.948\ 10^{-5}$	$\mu N\ \mu s/\mu m$
$\boldsymbol{\mu_2}$	$3.916\ 10^{-5}$	$\mu N\ \mu s\ /\mu m$

Table 2: Coefficients of the simplified analytical model.

A very good agreement between the two models is found in the quasi-periodic region, while small discrepancies are evident at high amplitudes. This is justified by the simplifying hypotheses adopted in the analytical model that does not take into account nonlinearities of higher orders, which are known to play a quantitative role at large amplitudes.

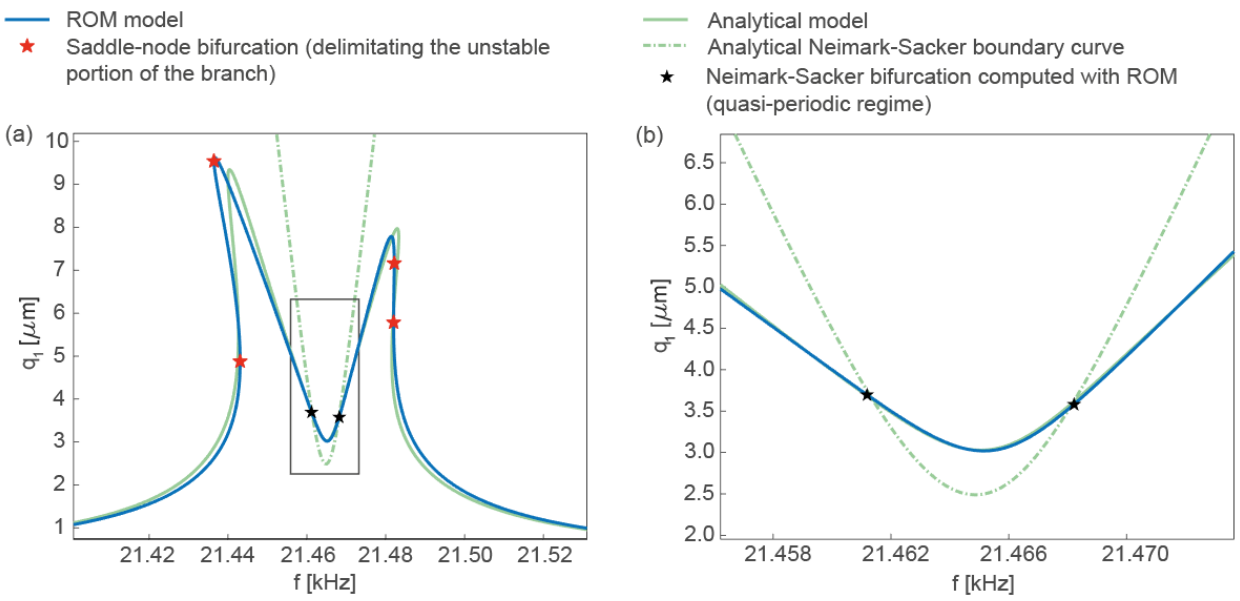

Figure 3: (a) Frequency response of the MEMS gyroscope test-structure for a V_{AC} = 3.16mV and a V_{DC} =4.28V. Comparison between the full ROM model proposed in the paper and the simplified analytical model. (b) Close-up view of the quasi-periodic region of the frequency response.

References

1. H. K. Lee et al. Stable operation of MEMS oscillators far above the critical vibration amplitude in the nonlinear regime, *J. Microelectromech. Syst*. **20**(6) 1228-1230 (2011).
2. G. Gobat et al Backbone Curves, Neimark-Sacker Boundaries and Appearance of Quasi-Periodicity in Nonlinear Oscillators: Application to 1:2 Internal Resonance and Frequency Combs in MEMS *Meccanica* (2021) doi: 10.1007/s11012-021-01351-1

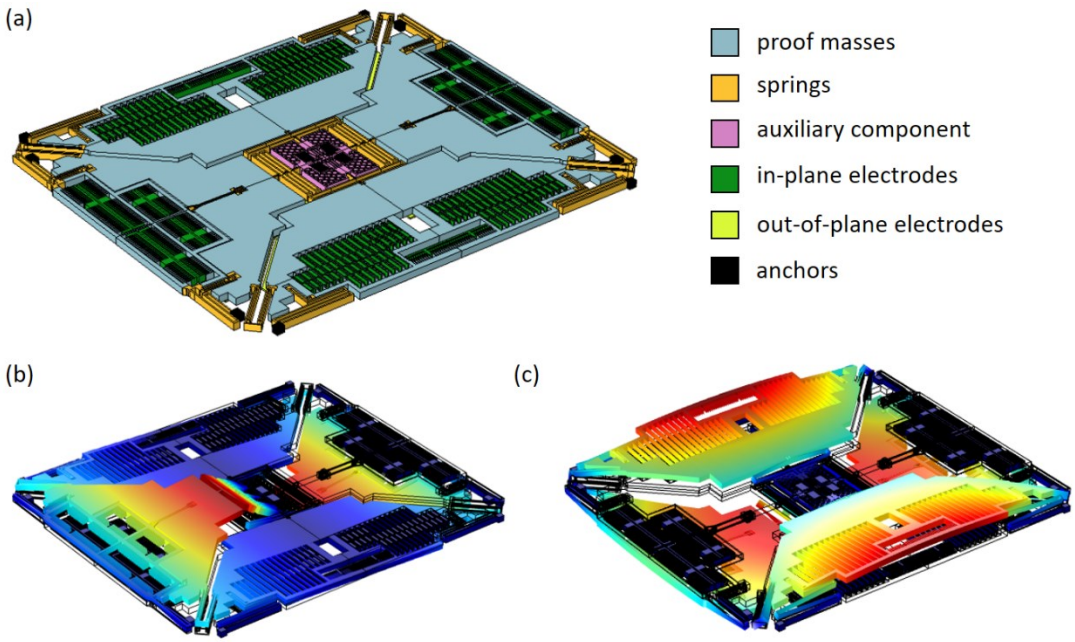

Figure 1: (a) Schematic view of the MEMS gyroscope test-structure. (b) Roll ($\boldsymbol{f_1}$ = 22522 Hz) and (c) spurious roll ($\boldsymbol{f_2}$ = 43386 Hz) modes. The contour plot of the displacement field is shown in color.

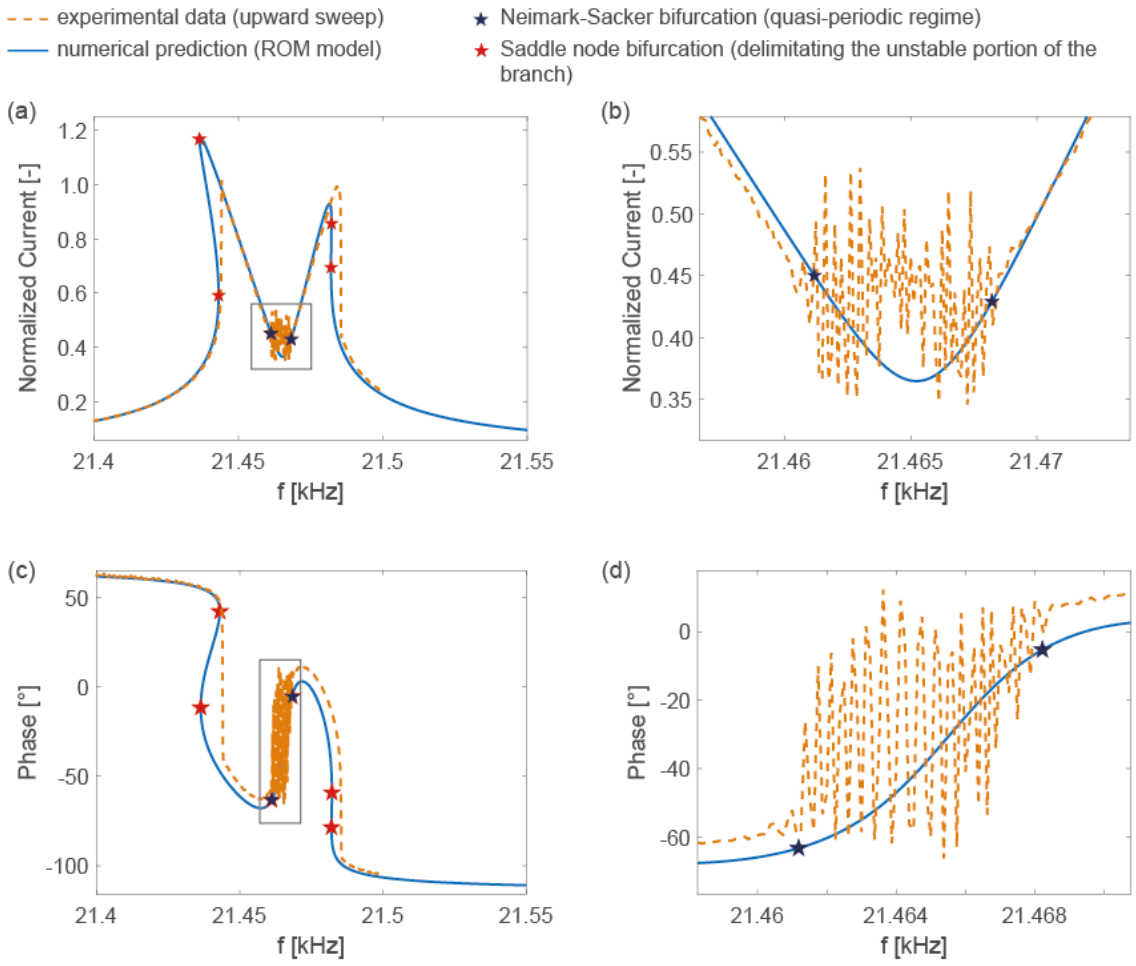

Figure 2: Frequency response of the MEMS gyroscope test-structure for a V_{AC} = 3.16mV and a V_{DC} =4.28 V in terms of (a) amplitude and (c) phase. Close-up views of the quasi-periodic region in the frequency response in terms of amplitude and phase are shown in (b)-(d). Numerical predictions are plotted with continuous blue lines, and experimental data with orange dashed lines. Stars mark theoretical Neimark-Sacker (dark blue) and Saddle-Node (red) bifurcations that delimit the quasi-periodic regime region and the unstable paths of the frequency response, respectively.

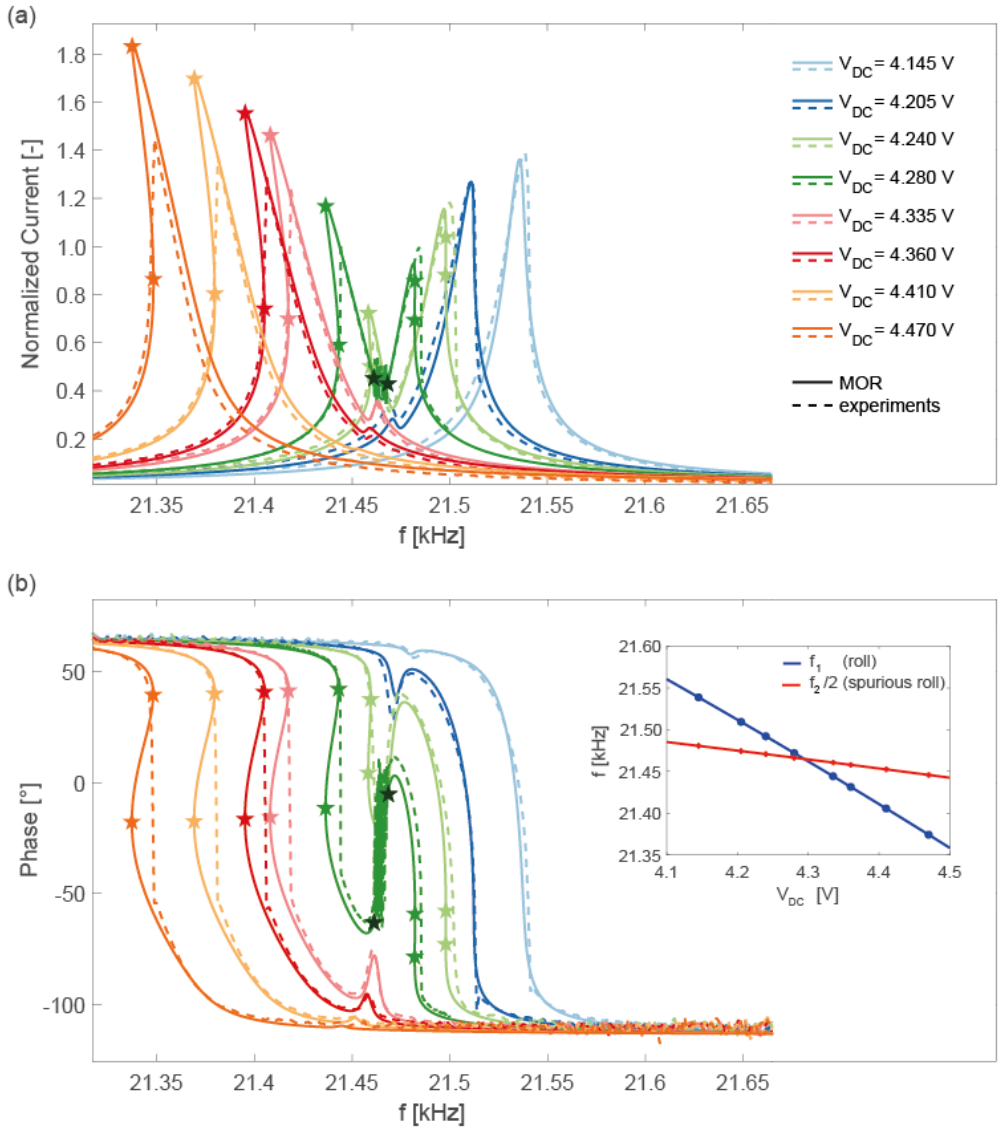

Figure 3: Frequency responses of the MEMS gyroscope test-structure for V_{AC} = 3.16mV and different levels of V_{DC} in terms of (a) amplitude and (b) phase. Numerical predictions are reported in continuous lines while experiments are in dotted lines. Stars of the same color of the curves mark the Saddle-Node bifurcations estimated through the ROM model, while black stars mark the Neimark-Sacker bifurcations that delimit the quasi-periodic region of the curves at V_{DC} = 4.28V. The resonant frequency of the roll mode ($\boldsymbol{f_1}$) and half of the resonant frequency of the spurious roll mode ($\boldsymbol{f_2/2}$) are reported in the inset for different V_{DC}.

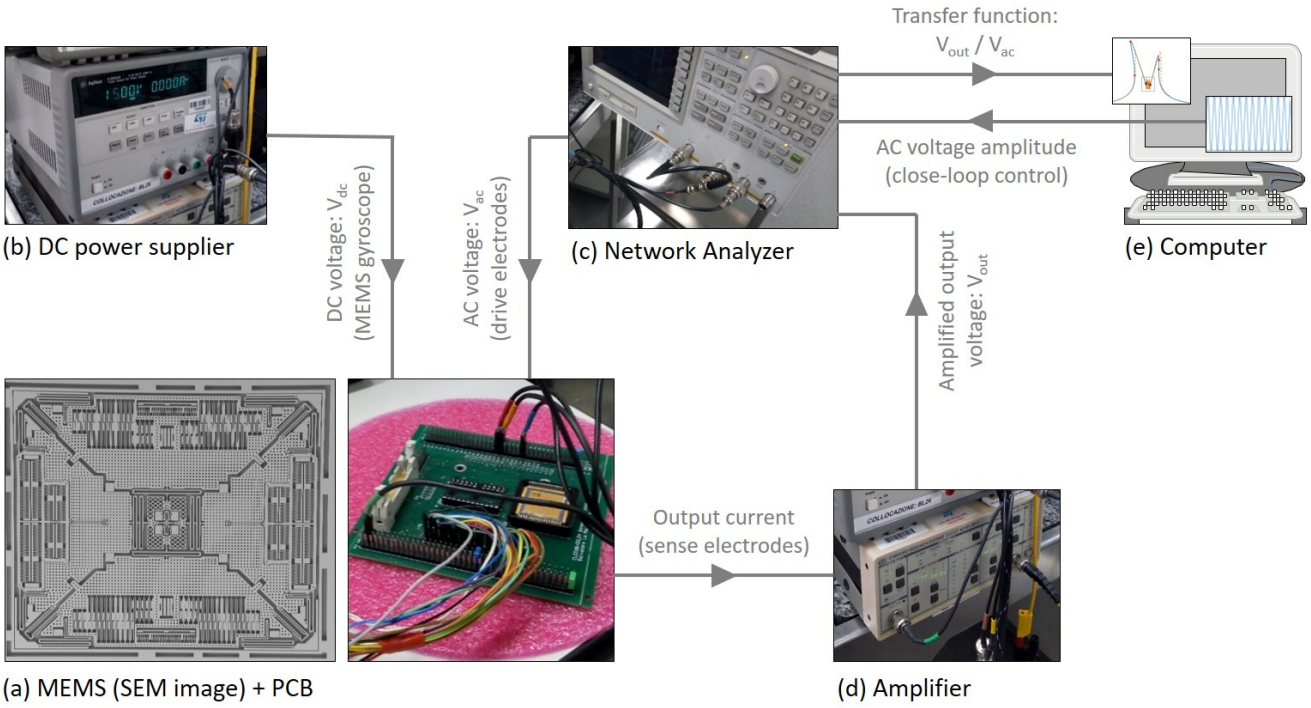

Figure 4: Set-up employed to measure experimental frequency responses.